

Cancellation of atmospheric turbulence effects in entangled two-photon beams

M. V. da Cunha Pereira, L. A. P. Filpi and C. H. Monken*

Departamento de Física, Universidade Federal de Minas Gerais, Caixa Postal 702,
Belo Horizonte, MG 30123-970, Brazil

*Corresponding author: monken@fisica.ufmg.br

Abstract: Turbulent airflow in the atmosphere and the resulting random fluctuations in its refractive index have long been known as a major cause of image deterioration in astronomical imaging and figures among the obstacles for reliable optical communication when information is encoded in the spatial profile of a laser beam. Here we show that using correlation imaging and a suitably prepared source of photon pairs, the most severe of the disturbances inflicted on the beam by turbulence can be cancelled out. Other than a two-photon light source, only linear passive optical elements are needed and, as opposed to adaptive optics techniques, our scheme does not rely on active wavefront correction.

© 2018 Optical Society of America

OCIS codes: (010.1300) Atmospheric propagation; (270.5565) Quantum communications

References and links

1. Larry C. Andrews and Ronald L. Phillips. *Laser beam propagation through random media*. SPIE press, 2005.
2. R.L. Fante. Electromagnetic beam propagation in turbulent media. *Proceedings of the IEEE*, 63(12):1669–1692, dec. 1975.
3. Alessandro Fedrizzi, Rupert Ursin, Thomas Herbst, Matteo Nespola, Robert Prevedel, Thomas Scheidl, Felix Tiefenbacher, Thomas Jennewein, and Anton Zeilinger. High-fidelity transmission of entanglement over a high-loss free-space channel. *Nat Phys*, 5(6):389–392, June 2009.
4. Gabriel Molina-Terriza, Juan P. Torres, and Lluís Torner. Management of the angular momentum of light: Preparation of photons in multidimensional vector states of angular momentum. *Phys. Rev. Lett.*, 88(1):013601–, December 2001.
5. Graham Gibson, Johannes Courtial, Miles Padgett, Mikhail Vasnetsov, Valeriy Pas’ko, Stephen Barnett, and Sonja Franke-Arnold. Free-space information transfer using light beams carrying orbital angular momentum. *Opt. Express*, 12(22):5448–5456, November 2004.
6. Leonardo Neves, G. Lima, J. G. Aguirre Gómez, C. H. Monken, C. Saavedra, and S. Pádua. Generation of entangled states of qudits using twin photons. *Phys. Rev. Lett.*, 94(10):100501–, March 2005.
7. J. B. Pors, S. S. R. Oemrawsingh, A. Aiello, M. P. van Exter, E. R. Eliel, G. W. ’t Hooft, and J. P. Woerdman. Shannon dimensionality of quantum channels and its application to photon entanglement. *Phys. Rev. Lett.*, 101(12):120502–, September 2008.
8. S.P. Walborn, C.H. Monken, S. Pádua, and P.H. Souto Ribeiro. Spatial correlations in parametric down-conversion. *Physics Reports*, 495(4-5):87–139, October 2010.
9. Jian Wang, Jeng-Yuan Yang, Irfan M. Fazal, Nisar Ahmed, Yan Yan, Hao Huang, Yongxiong Ren, Yang Yue, Samuel Dolinar, Moshe Tur, and Alan E. Willner. Terabit free-space data transmission employing orbital angular momentum multiplexing. *Nat Photon*, 6(7):488–496, July 2012.
10. Sebastian Randel, Roland Ryf, Alberto Sierra, Peter J. Winzer, Alan H. Gnauck, Cristian A. Bolle, René-Jean Essiambre, David W. Peckham, Alan McCurdy, and Robert Lingle. 6×56-Gb/s mode-division multiplexed transmission over 33-km few-mode fiber enabled by 6×6 MIMO equalization. *Opt. Express*, 19(17):16697–16707, August 2011.
11. C. Paterson. Atmospheric turbulence and orbital angular momentum of single photons for optical communication. *Phys. Rev. Lett.*, 94(15):153901–, April 2005.
12. Mehul Malik, Malcolm O’Sullivan, Brandon Rodenburg, Mohammad Mirhosseini, Jonathan Leach, Martin P. J. Lavery, Miles J. Padgett, and Robert W. Boyd. Influence of atmospheric turbulence on optical communications using orbital angular momentum for encoding. *Opt. Express*, 20(12):13195–13200, June 2012.
13. Maged B. Nasr, Bahaa E. A. Saleh, Alexander V. Sergienko, and Malvin C. Teich. Demonstration of dispersion-canceled quantum-optical coherence tomography. *Phys. Rev. Lett.*, 91(8):083601–, August 2003.
14. Cristian Bonato, Alexander V. Sergienko, Bahaa E. A. Saleh, Stefano Bonora, and Paolo Villorosi. Even-order aberration cancellation in quantum interferometry. *Phys. Rev. Lett.*, 101(23):233603–, December 2008.
15. D. S. Simon and A. V. Sergienko. Spatial-dispersion cancellation in quantum interferometry. *Phys. Rev. A*, 80(5):053813–, November 2009.

16. Kam Wai Clifford Chan, D. S. Simon, A. V. Sergienko, Nicholas D. Hardy, Jeffrey H. Shapiro, P. Ben Dixon, Gregory A. Howland, John C. Howell, Joseph H. Eberly, Malcolm N. O’Sullivan, Brandon Rodenburg, and Robert W. Boyd. Theoretical analysis of quantum ghost imaging through turbulence. *Phys. Rev. A*, 84(4):043807–, October 2011.
17. P. Ben Dixon, Gregory A. Howland, Kam Wai Clifford Chan, Colin O’Sullivan-Hale, Brandon Rodenburg, Nicholas D. Hardy, Jeffrey H. Shapiro, D. S. Simon, A. V. Sergienko, R. W. Boyd, and John C. Howell. Quantum ghost imaging through turbulence. *Phys. Rev. A*, 83(5):051803–, May 2011.
18. David S. Simon and Alexander V. Sergienko. Turbulence mitigation in phase-conjugated two-photon imaging. May 2011.
19. R. Prevedel, Y. Lu, W. Matthews, R. Kaltenbaeck, and K. J. Resch. Entanglement-enhanced classical communication over a noisy classical channel. *Phys. Rev. Lett.*, 106(11):110505–, March 2011.
20. D. L. Fried. Statistics of a geometric representation of wavefront distortion. *J. Opt. Soc. Am.*, 55(11):1427–1431, November 1965.
21. D. L. Fried. Optical resolution through a randomly inhomogeneous medium for very long and very short exposures. *J. Opt. Soc. Am.*, 56(10):1372–1379, October 1966.
22. Onur Keskin, Laurent Jolissaint, and Colin Bradley. Hot-air optical turbulence generator for the testing of adaptive optics systems: principles and characterization. *Appl. Opt.*, 45(20):4888–4897, July 2006.
23. J. W. Strohbehn, S. F. Clifford, M. E. Gracheva, A. S. Gurvich, S. S. Kashkarov, V. V. Pokasov, A. Ishimaru, J. H. Shapiro, J. L. Walsh, and P. B. Ulrich and. *Laser Beam Propagation in the Atmosphere*, volume 25 of *Topics in Applied Physics*. Springer-Verlag, 1978.
24. Jason D. Schmidt. *Numerical Simulation of Optical Wave Propagation with examples in MATLAB*. SPIE press, pap/chrt edition, August 2010.
25. Ryan S. Bennink, Sean J. Bentley, and Robert W. Boyd. "Two-photon" coincidence imaging with a classical source. *Phys. Rev. Lett.*, 89(11):113601–, August 2002.
26. Ryan S. Bennink, Sean J. Bentley, Robert W. Boyd, and John C. Howell. Quantum and classical coincidence imaging. *Phys. Rev. Lett.*, 92(3):033601–, January 2004.
27. M. V. Fedorov, M. A. Efremov, P. A. Volkov, E. V. Moreva, S. S. Straupe, and S. P. Kulik. Anisotropically and high entanglement of biphoton states generated in spontaneous parametric down-conversion. *Phys. Rev. Lett.*, 99(6):063901–, August 2007.

1. Introduction

Fluctuations of the atmospheric refractive index due to turbulent air flow have long been known as a major cause of image deterioration in astronomical imaging. Such fluctuations figure among the main obstacles to reliable optical communication [1], by causing signal attenuation and distortion. One possible way to avoid turbulence effects in optical communications is to encode information in the polarization degree of freedom, since it is well known that polarization is marginally affected by clear air propagation disturbances [2, 3]. However, due to the two-dimensional nature of polarization states, the amount of information carried by a single pulse is limited to one bit, or to one qubit per photon in the quantum case. On the other hand, transverse spatial degrees of freedom of higher-order beams allow for spaces of much larger dimensionality to be accessed [4, 5, 6, 7, 8, 9], and these have been gaining prominence even in optical fiber communications, through the use of few-mode fibers and spatial division multiplexing for increased communication capacity[10]. In the case of free-space (not vacuum) propagation however, there is the problem that information encoded in photonic spatial degrees of freedom are typically severely degraded by atmospheric turbulence [11, 12].

Entanglement has been exploited in numerous situations to cancel unwanted effects such as group-velocity dispersion [13], spatial aberrations and dispersion [14, 15, 16, 17] and, with the use of a phase-conjugating mirror, a proposal has been made even to mitigate atmospheric turbulence phase distortions [18]. It has also been recently shown in ref. [19] that the strong correlations observed in entangled states can assist in performing classical communication under the effect of specific sources of error. We show here a new scheme that does not resort to active compensation but, with the aid of the correlations present in a spontaneous parametric down-conversion (SPDC) source, makes spatial information immune to all odd-order spatial aberrations (both in amplitude and phase) caused by refractive index fluctuations in the atmosphere. Among these is the wavefront tilt, which has long been known [20] for being the most deleterious in terms of loss in resolution when long-exposure imaging is used [21], accounting for as much as 80% of the total wavefront distortion [1].

2. Theory

Our basic scenario (see fig 2) is a two-photon light beam of wavenumber k generated by collinear type I SPDC propagating horizontally in the z direction, impinging on a receiver

(detector) of aperture A located at a distance L from the transmitter (the nonlinear crystal). Throughout the propagation path, the field undergoes the effects of atmospheric turbulence (refractive index fluctuations). The SPDC pump beam is a laser beam of wavenumber $k_p = 2k$, focused on A . The two-photon state generated by collinear type I SPDC, neglecting birefringence effects in the nonlinear crystal, in the monochromatic and paraxial approximations is proportional to [8]

$$\int d^2 q_1 \int d^2 q_2 \mathcal{E}_p(q_1 + q_2) \text{sinc } \beta |q_1 - q_2|^2 |q_1\rangle |q_2\rangle, \quad (1)$$

where q_1 and q_2 are the transverse (xy) components of the down-converted wave vectors, \mathcal{E}_p is the pump beam plane wave spectrum, $\beta = \tau/4k_p$, τ is the nonlinear crystal thickness, and $|q_1\rangle$ and $|q_2\rangle$ are one-photon states in plane wave modes defined by q_1 and q_2 . This state gives rise to the following two-photon detection amplitude at the point $r_1 = r_2 = r = (\rho, L\hat{z})$:

$$\mathcal{A}^{(2)}(r, r) \propto \int d^2 \rho'_1 \int d^2 \rho'_2 E_p \left(\frac{\rho'_1 + \rho'_2}{2} \right) V(\rho'_1 - \rho'_2) \exp \left[\frac{ik}{2L} (|\rho'_1 - \rho|^2 + |\rho'_2 - \rho|^2) \right], \quad (2)$$

where E_p is the Fourier transform of \mathcal{E}_p , that is, pump beam profile on the $z = 0$ plane (nonlinear crystal) and V is the Fourier transform of the sinc function.

In the presence of turbulence, we have to include complex random phase factors ψ for each down-converted photon in (2), which leads to

$$\begin{aligned} \mathcal{A}_T^{(2)}(r, r) \propto & \int d^2 \rho'_1 \int d^2 \rho'_2 E_p \left(\frac{\rho'_1 + \rho'_2}{2} \right) V(\rho'_1 - \rho'_2) \exp \left[\frac{ik}{2L} (|\rho'_1 - \rho|^2 + |\rho'_2 - \rho|^2) \right] \\ & \times \exp [\psi(\rho'_1, \rho; k) + \psi(\rho'_2, \rho; k)], \end{aligned} \quad (3)$$

where each complex phase factor $\psi(\rho', \rho; k)$ represents a random distortion, both in phase and amplitude, of a spherical wave with wavenumber k originated in ρ' on the source plane, and observed in ρ on the observation plane ($z = L$). If we consider that the nonlinear crystal is thin enough (typically, a few millimeters), the sinc function in Eq. (1) is broad in $q_1 - q_2$ and its Fourier transform V can be approximated by a delta function $\delta(\rho'_1 - \rho'_2)$. Then, $\mathcal{A}_T^{(2)}$ can be approximated by

$$\mathcal{A}_T^{(2)}(r, r) \propto \int d^2 \rho' E_p(\rho') \exp \left[\frac{ik_p}{2L} |\rho' - \rho|^2 \right] \exp [\psi(\rho', \rho; k_p)], \quad (4)$$

where in the passage from (3) to (4) we used the fact that $k_p = 2k$ and $2\psi(\rho', \rho; k) = \psi(\rho', \rho; k_p)$, neglecting dispersion. From Eq. (4) it is clear that the two-photon beam under turbulence behaves like the pump beam would in the same conditions.

We now show that the effects of turbulence can be mitigated if we make a coordinate inversion in one of the photons: $q_2 \rightarrow -q_2$ and calculate the two-photon detection amplitude at the points $r_1 = r = (\rho, L\hat{z})$ and $r_2 = \tilde{r} = (-\rho, L\hat{z})$. All the steps above can be repeated, leading to

$$\mathcal{A}_T^{(2)}(r, \tilde{r}) \propto \int d^2 \rho' E_p(\rho') \exp \left[\frac{ik_p}{2L} |\rho' - \rho|^2 \right] \exp [\psi(\rho', \rho; k) + \psi(-\rho', -\rho; k)]. \quad (5)$$

One can see from Eq. (5) that the total perturbation is now symmetric with respect to the z axis, that is to say, the antisymmetric part of ψ is cancelled out. In particular, wavefront tilt, modeled by $\psi_t(\rho', \rho; k) = (ik/2L)(\rho' - \rho) \cdot d$, where d is a random displacement, can be seen to vanish in Eq. (5). It is imperative for the cancellation to happen that the correlated photons propagate near-collinearly and close enough so that the random process describing turbulence ψ is the same for both.

3. Experiment

To emulate the conditions present in the real atmosphere we adapted a tabletop turbulence generator put forward by Keskin [22], depicted in figure 1. Cold and hot air fluxes are mixed inside an aluminum box, resulting in a random temperature field. Consequently, the refractive index inside the box fluctuates in both space and time [23]. Air is blown into the chamber by two

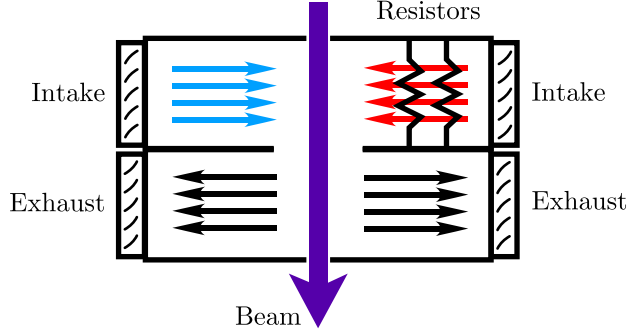


Fig. 1. (color online). A turbulence chamber that emulates the turbulent mixing of air at different temperatures in the atmosphere.

fans, one of them having a resistor bank (6.4Ω) in front of it, which is driven by an adjustable power supply to dissipate up to 200 W. Two other fans work as exhausts, to ensure that the process is stationary. Each dissipated power corresponds to a different turbulence strength, which we characterize as follows: we expand and then focus a He-Ne laser beam with a lens system onto a charge-coupled device (CCD) camera, placed at a distance of 93 cm from the output lens. The beam has a wavenumber $k_l = 2\pi/0.633 = 9.93 \mu\text{m}^{-1}$ and waist (e^{-2} radius on the detection plane) $w_0 = 58.3 \mu\text{m}$. The turbulence chamber, positioned halfway between the beam expander and the CCD, causes the beam spot to undergo a random motion and distortion. All long-term average (over 55 s) transverse profiles remain Gaussian in shape, yet with a radius w_{LT} , which increases according to [1]

$$w_{LT}^2 = w_0^2 \left(1 + \frac{k_l^{1/3}}{w_0^{5/3}} \gamma^2 \right). \quad (6)$$

Turbulence strength can be thus characterized by $\gamma = [7.75L^{5/3} \int_0^L C_n^2(z) (1 - z/L)^{5/3} dz]^{1/2}$, where C_n^2 is the refractive index structure constant. The parameter γ is closely related to the more commonly used Rytov variance $\sigma_R^2 = 1.23C_n^2 k_l^{7/6} L^{11/6} = 0.423k_l^{7/6} L^{-5/6} \gamma^2$ when C_n^2 is constant through the propagation path. Kolmogorov spectrum for the refractive index spatial fluctuations $\Phi_n(\kappa) = 0.033C_n^2 \kappa^{-11/3}$ is assumed in the derivation of Eq. (6) [1]. Equation (6) allows us to determine γ for each measured dissipated power as shown in Table I.

Power (W)	$w_{LT}(\mu\text{m})$	$\gamma(\mu\text{m})$
0	58.3	0
16.0	59.6	4.29
34.5	62.7	7.99
60.0	68.0	12.1
95.0	75.4	16.6
135.0	84.7	21.3
185.5	99.5	27.9

Table 1. Calibration of the turbulence chamber. The parameter γ is listed as a function of the power dissipated by the resistors.

The experimental verification of expressions (4) and (5) was made in two steps, which we refer to as first experiment and second experiment, respectively. The setup is depicted in Fig. 2. A two-photon beam with wavelength of 650 nm is produced by degenerate spontaneous parametric down-conversion in a 5 mm long BiB_3O_6 (BiBO) nonlinear crystal (NL), such that the two-photon (coincidence) detection profile on the detection aperture S is a Gaussian whose width is $60 \mu\text{m}$, whereas the single-photon (intensity) profile width is of the order of 10 mm. The detection aperture is a $50 \mu\text{m}$ -wide slit oriented vertically. We note that refractive index fluctuations in air have spatial scales exceeding a millimeter [2], so that for $\rho < 50 \mu\text{m}$, the complex phase factors in Eq. (5) satisfy $\psi(\rho', \rho; k) \approx \psi(\rho', 0; k)$, and cancellation still effectively follows as if we were using point detectors centered in $\rho = 0$. The detectors are avalanche

photodiodes operating in photon counting mode with a coincidence resolving time of 5 ns. Interference band-pass filters centered at 650 nm with 10 nm bandwidth and coupling microscope objectives are used in front of each detector.

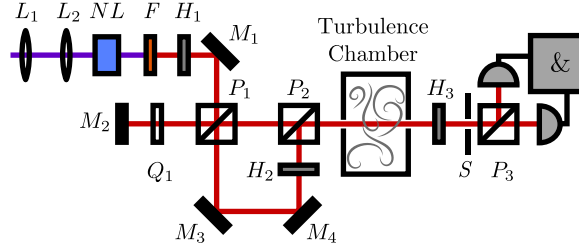


Fig. 2. (color online). **Experimental setup.** The two-photon source consists of the lens set L_1 , L_2 , the nonlinear crystal NL and the uv filter F . The arrangement of optical elements from H_1 to H_3 is responsible for the control of coordinate inversion of one photon (see text). The detection system consists of an aperture S , a polarizing beam-splitter P_3 and two photon counters.

In the first experiment, all photons are made to propagate through the same path of an interferometer-like arrangement, so that the coincidence rate is described by Eq. (4), while in the second experiment all coincidence events correspond to each photon of a pair going through different arms. The arrangement is made such that there is an additional reflection in one of the arms, resulting in the momentum inversion necessary to obtain the conditions leading to Eq. (5). To switch between these configurations, the polarization of the photon pairs can be rotated before or after the turbulence to 45 degrees with respect to the horizontal plane, by means of two half-wave plates (HWP) H_1 and H_3 .

When H_1 is set to 0° , all photon pairs are reflected by the polarizing beam-splitter (PBS) P_1 , back reflected with horizontal polarization by the combination of a quarter-wave plate Q_1 and a mirror M_2 , and transmitted by PBS P_2 . After crossing the turbulence chamber, the photon pairs have their polarization rotated to 45° by HWP H_3 and are split by PBS P_3 with probability $1/2$. The split events are registered as coincidence counts. This situation corresponds to the first experiment.

For the second experiment, HWP H_1 rotates the photon polarizations to 45° so that the photon pairs are split by P_1 with probability $1/2$. The HWP H_2 in the bottom arm rotates the polarization from horizontal to vertical, so that all photons leave P_2 going towards the turbulence chamber. Because H_3 is now set to 0° , only the cases where the photon pairs are split by P_1 give rise to coincidence counts. Since a photon going through the bottom arm undergoes an additional horizontal reflection, a coordinate inversion is effected on the horizontal plane.

Distortions and beam deflections make the averaged coincidence transverse profile larger at the aperture plane and, because of the small width of the slit, the signal decreases. Results are shown in Fig. 3, with normalized detection counts plotted against the turbulence strength, as measured by the parameter γ . Absolute coincidence rates without turbulence ($\gamma = 0$) are 75 and 78 counts per second in the first and second experiments, respectively. We also included the measurements done with the He-Ne laser used to calibrate γ and with the pump He-Cd laser. In this latter measurement, the laser beam was focused down to a waist radius of $58 \mu\text{m}$ onto a CCD, where the slit was previously positioned, as it was done with the He-Ne laser. For both the He-Ne and He-Cd measurements, we mimicked the $50 \mu\text{m}$ slit by integrating the gray level value over a region of interest defined by a vertical stripe 11 pixels wide in the CCD camera (which amounts to $51 \mu\text{m}$). In both coincidence data sets (blue circles and green squares), each point is the result of an average over 100 samples of coincidence counts with a sampling time of 5 s, while for the He-Ne and He-Cd measurements (red triangles and purple diamonds) we recorded 11 sample videos of 5 s each. The error bars are the standard deviations over the samples. One can immediately see that the coincidences without inversion and pump beams perform rather similarly under turbulence, as expected from Eq. (4).

The plot is separated by a vertical dashed line into two distinct regions. The left and right parts correspond to the weak and strong turbulence regimes for the He-Ne laser, respectively. The separating line is defined by the value of γ such that $k_l^{1/3} w_0^{-5/3} \times \gamma^2 \approx 1.33$, and delimits

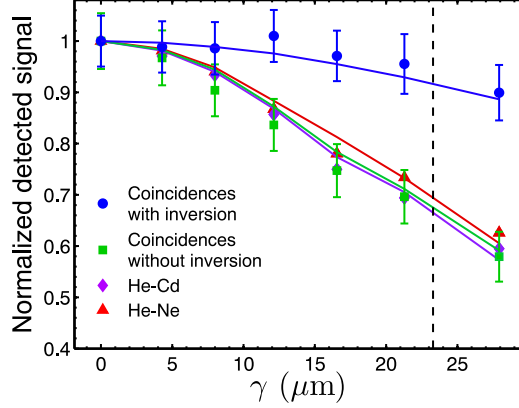


Fig. 3. (color online). **Experimental results.** Normalized detection counts plotted against turbulence strength as measured by γ . Plot markers and solid lines represent measured and simulated values, respectively. Blue circles: Normalized coincidence counts when the x coordinate of one photon is inverted. Green squares: normalized coincidence counts with no coordinate transformation. Purple diamonds: integrated gray levels of the He-Cd laser long-term average intensity profiles in a $50 \mu\text{m}$ wide region of the CCD camera. Red triangles: Values used for the calibration of γ . Same procedure as for the He-Cd, but with the He-Ne laser.

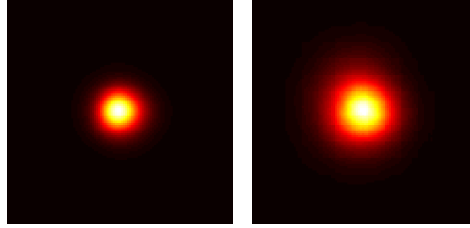


Fig. 4. Averaged He-Cd beam profile with and without tilt correction.

the turbulence strength above which the scintillation index exceeds unity [1].

To test our model, a Monte Carlo simulation was performed using randomly generated phase screens, along the lines of Ref. [24], and using equations (4) and (5) to describe propagation of the coincidence beams. The resulting curves are shown in Fig. 3. Again, Kolmogorov spectrum was assumed, along with turbulence strength homogeneity inside the chamber, leaving only the number of phase screens and their separation as free parameters; we chose these to be the same for all curves. While there are some discrepancies, which we tentatively attribute to differences between the refractive index statistics in our turbulence chamber and that of the atmosphere, the normalized power increase in the inverted coincidence beam scenario closely matches what was measured.

Additionally, curve fits (not shown) were performed on the data by considering the Gaussian width to broaden according to $w_{LT} = w_0 \left[1 + \alpha(k^{1/3}/w_0^{5/3})\gamma^2 \right]^{1/2}$ with k and w_0 corresponding to each data set. The fit parameter α can be interpreted as the effective turbulence response and provides us with a figure of merit. The total signal going through the aperture is then $S_L(\gamma) = \text{erf}\left(\frac{a}{\sqrt{2}w_{LT}}\right)$ for the laser measurements, $a = 50 \mu\text{m}$ being the slit width, and $S_C(\gamma) = 1/w_{LT} \int_{-\infty}^{\infty} \exp(-2x^2/w_{LT}^2) \Lambda(2x/a) dx$ for the coincidence measurements, where $\Lambda(x) = 1 - |x|$ for $|x| < 1$ and 0 otherwise [8]. The fitted curves are therefore $S_L(\gamma)/S_L(0)$ and $S_C(\gamma)/S_C(0)$.

An additional test was performed by correcting both lasers for wavefront tilt, via post-processing. This is done by displacing the beam spot transversely in each frame of the recorded video so that its centroid always falls on the same position, before taking the average over the frames. The pictures in Fig. 4 show the improvement with this correction applied to the He-Cd beam for $\gamma = 27.9 \mu\text{m}$ (maximum turbulence strength). All fit parameters α , including the ones corresponding to tilt-corrected data, are shown on Table II.

Setup	α
Coincidences with inversion	0.10 ± 0.03
Coincidences without inversion	1.01 ± 0.11
He-Cd without correction	1.02 ± 0.08
He-Ne without correction	1.07 ± 0.09
Corrected He-Cd	0.21 ± 0.02
Corrected He-Ne	0.30 ± 0.04

Table 2. Fit parameters α corresponding to the different setups (see text).

The ratios between α for the corrected and uncorrected lasers (0.21 ± 0.03 and 0.28 ± 0.04 for He-Cd and He-Ne) agree reasonably well with the value of 0.25 from models found in the literature [1]. It is to be noticed that although a significant improvement can be made just by correcting wavefront tilt (80% for the He-Cd and 71% for the He-Ne), it is not as significant as the improvement reached with the inversion on the coincidence beam (90%), thus providing further support to the claim that aberrations other than tilt are being corrected.

4. Conclusion

An interesting question that naturally arises is whether entanglement is actually necessary to attain the cancellation effect observed. In Ref. [25] it is demonstrated that for a known transfer function, classical correlations can be engineered in such a way as to reproduce any joint detection probability attainable in a single plane with entangled photons. Since the channel transfer function changes in an unpredictable way because of turbulence, it would need to be continuously monitored in order to have its form determined, in the same lines of adaptive optics. In our case, the necessary conditions are the transfer of angular spectrum from the pump beam to the down-converted two-photon field, which allows for the control of the spatial correlations in the far field, associated with a strong (δ -like) spatial correlation of the two photons on the source plane. Control of correlations in both far and near fields is naturally limited with separable two-photon sources [26]. Moreover, in order to take practical advantage of the effect reported here, the single-count rate or intensity transverse profile observed on the detection plane must be much broader than the coincidence rate profile. Since the ratio between the single and coincidence count profile widths gives a good estimate for the Schmidt number of the two-photon state entangled in spatial modes [27], our scheme would work well only for highly entangled states. In this sense, our results suggest that spatial mode entanglement can be protected against turbulence when two-photon states are transmitted through the atmosphere.

Acknowledgements

We acknowledge the support from the Brazilian funding agencies CNPq, CAPES and FAPEMIG.